

# EHands: Quantum Protocol for Polynomial Computation on Real-Valued Encoded States

Jan Balewski,<sup>1</sup> Mercy G. Amankwah,<sup>2</sup> E. Wes Bethel,<sup>3</sup> Talita Perciano,<sup>4,\*</sup> and Roel Van Beeumen<sup>5,\*</sup>

<sup>1</sup>*National Energy Research Scientific Computing Center,  
Lawrence Berkeley National Laboratory, Berkeley, CA 94720, USA*

<sup>2</sup>*Department of Mathematics, Applied Mathematics and Statistics,  
Case Western Reserve University, Cleveland, OH 44106, USA*

<sup>3</sup>*Computer Science Department, San Francisco State University, San Francisco, CA 94132, USA*

<sup>4</sup>*Scientific Data Division, Lawrence Berkeley National Laboratory, Berkeley, CA 94720, USA*

<sup>5</sup>*Applied Mathematics and Computational Research Division,  
Lawrence Berkeley National Laboratory, Berkeley, CA 94720, USA*

(Dated: February 25, 2025)

The novel constructive **EHands protocol** defines a universal set of quantum operations for multivariable polynomial transformations on quantum processors by introducing four basic subcircuits—*multiplication*, *addition*, *negation*, and *parity flip*—and by using expectation-value encoding (EVEN) to represent real numbers in quantum states. These elementary arithmetic operations can be systematically composed to compute degree- $d$  polynomials,  $P_d(x)$ , on a QPU. The resulting quantum circuit structure closely mirrors the stepwise evaluation of polynomials on a classical calculator, providing an intuitive and efficient approach to polynomial computation on quantum hardware. By enabling direct, predictable polynomial and nonlinear data transformations on a QPU, our method reduces dependence on classical post-processing in hybrid quantum-classical algorithms, enabling advancements in many quantum algorithms. The **EHands** quantum circuits are compact enough to deliver meaningful and accurate results on today’s noisy quantum processors. We present a detailed implementation of  $P_d(x)$  and report experimental results for polynomial approximations of common functions, obtained using IBM’s Heron-class quantum processors and an ideal Qiskit simulator.

## I. INTRODUCTION

Quantum computing promises to accelerate computation across a wide range of scientific disciplines, driving the development of numerous quantum algorithms with provable advantages. Significant breakthroughs include Shor’s algorithm for factoring large numbers [1], Grover’s search algorithm for efficient database querying [2], and the HHL method for solving systems of linear equations [3].

While some quantum algorithms, such as quantum dynamics simulation [4], naturally map to quantum computers, classical computers remain superior in executing arithmetic operations with high precision and efficiency. Developing efficient quantum algorithms for fundamental arithmetic operations, such as addition, multiplication, and exponentiation, is crucial for the broader adoption of quantum computing. These capabilities would enable end-to-end quantum computation by eliminating the cyclic collapse of the quantum state, removing the need for classical processing of quantum measurements, and avoiding repeated quantum state reinitialization, which are major bottlenecks in hybrid quantum-classical approaches.

Polynomial transformations are essential for various scientific and engineering applications, including interpolation and approximation of non-linear functions. Ef-

ficient implementation of these operations on quantum processing units (QPUs) is critical for unlocking their computational advantages. However, existing quantum algorithms for polynomial transformations remain underdeveloped, often mimicking classical techniques, using discretized inputs, and relying on binary encoding schemes [5–9]. These approaches typically require numerous ancilla qubits or deep quantum circuits, making them impractical for near-term quantum hardware.

Alternative methods, such as quantum signal processing (QSP) [10, 11], quantum singular value transformation (QSVT) [12], and quantum eigenvalue transformation (QET) [13], enable implicit polynomial transformations on singular values or eigenvalues. However, these techniques are not designed for direct polynomial evaluation on encoded input data, limiting their applicability for general-purpose polynomial transformations on QPUs. For completeness, we also mention hybrid approaches that iteratively tune a parameterized ansatz to approximate the desired function [14]. While these methods offer valuable insights, their practical feasibility on real quantum hardware remains uncertain.

In this paper, we introduce a *quantum-native protocol* for performing basic arithmetic operations, such as addition ( $a + b$ ) and multiplication ( $a \cdot b$ ). By eliminating the need for discretization, our approach utilizes shallow quantum circuits to execute these operations efficiently using only two qubits. For degree- $d$  polynomial transformations, our approach requires only  $d + 1$  qubits. It generates circuits with depth linear in  $d$ , which can be directly executed using elementary one- and two-qubit

\* Corresponding authors: [tperciano@lbl.gov](mailto:tperciano@lbl.gov), [rvanbeeumen@lbl.gov](mailto:rvanbeeumen@lbl.gov)

gates. To accomplish this, we propose a novel encoding scheme, Expectation Value ENcoding (EVEN), along with four elementary subcircuits—*addition*, *multiplication*, *negation*, and *parity flip*—which together constitute a universal set of quantum operations for multivariable polynomial transformations on QPUs.

## II. EXPECTATION-VALUE ENCODING (EVEN) SCHEME

We begin by introducing a novel scheme to *encode the input*, which consists of a list of  $N \geq 1$  real values  $x_i \in [-1, 1]$ . To achieve this, we construct a product state  $|\phi\rangle$  with  $N$  qubits, each initialized in the  $|0\rangle$  state and subjected to an  $R_y(\theta_i)$  rotation, where  $\theta_i = \arccos(x_i)$ .

To retrieve data from a specific qubit in the EVEN state  $|\phi\rangle$ , we apply *decoding* by measuring the expectation value (EV) of the Pauli- $Z$  operator for that qubit, given by  $\hat{x} = \langle \phi | O | \phi \rangle$ . [Figure 1a](#) shows the encoding and decoding of an EVEN state for a single real input  $x$ . See [Appendix A 1](#) for encoding and decoding of 2 real numbers on 2 qubits.

The EVEN scheme generally falls within the category of angle encoding [\[15\]](#). Its key distinction lies in the mapping process. Rather than using a simple linear transformation to convert a real number into a rotation angle within the range  $[0, \pi]$ , EVEN applies a non-linear transformation via the arccos function. This seemingly minor modification plays a crucial role in simplifying the polynomial transformation protocol described below.

## III. THE EHANDS PROTOCOL

We introduce four fundamental quantum operations: (1) *product-with-memory*, (2) *weighted sum*, (3) *negation*, and (4) *parity flip*. These operations will serve as the building blocks for polynomial calculations. [Figures 1b](#) to [1e](#) present their corresponding quantum circuits.

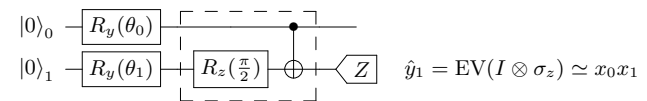
The **product-with-memory** operation is defined by the unitary  $U_{\text{prod}} = \text{CNOT}_{0,1} \cdot [I \otimes R_z(\pi/2)]$ . [Figure 1b](#) shows its implementation. For the pair of inputs  $x_0, x_1$ , the information about their product is stored in qubit  $q_1$ , while qubit  $q_0$  retains information about  $x_0$ . The value of  $x_0x_1$  can be retrieved by measuring the EV of the operator  $O_p = I \otimes \sigma_z$ . Alternatively, additional quantum operations can be applied to either qubit for further computations.

The **weighted sum** operation is defined by  $U_{\text{sum}}(w) = [R_y(-\alpha/2) \otimes I] \cdot \text{CNOT}_{1,0} \cdot [R_y(\alpha/2) \otimes I] \cdot U_{\text{prod}}$ , shown in [Fig. 1c](#). The parameter  $\alpha = \arccos(1 - 2w)$  depends on the chosen relative weight  $w \in [0, 1]$ , making  $U_{\text{sum}}(w)$  a parametric unitary operator. It computes the weighted sum  $S_w(x_0, x_1) = wx_0 + (1-w)x_1$ , with the result stored in qubit  $q_0$ . The estimator of  $S_w(x_0, x_1)$  can be retrieved by measuring the EV of the complementary operator  $O_s = \sigma_z \otimes I$ . Again, further arithmetic operations can

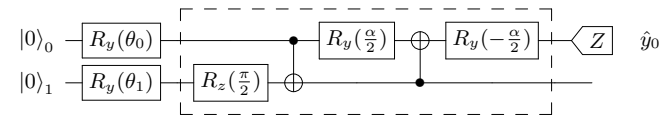
(a) EVEN encoding and decoding

$$|0\rangle \xrightarrow{R_y(\theta)} |\phi\rangle \rightarrow |\phi\rangle \xrightarrow{Z} \hat{y} = \text{EV}(\sigma_z) \simeq x$$

(b) product-with-memory (multiplication)



(c) weighted sum (addition)  $\hat{y}_0 = \text{EV}(\sigma_z \otimes I) \simeq wx_0 + (1-w)x_1$



(d) sign change (negation)

$$|0\rangle \xrightarrow{R_y(\theta)} \xrightarrow{X} \xrightarrow{Z} \hat{y} \simeq -x$$

(e) parity flip

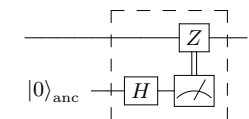


[FIG. 1.](#) (a) EVEN encoding of the real number  $x$  into the quantum state  $|\phi\rangle$  using  $\theta = \arccos(x)$ , along with its decoding, where the expectation value of the Pauli- $Z$  operator is the estimator  $\hat{x}$ . The four building blocks of the **EHANDS protocol**: (b) multiplication, (c) addition, (d) negation, and (e) random parity flip.

be performed on the data encoded in qubit  $q_0$ . Strictly speaking, the weighted sum circuit could also be used for multiplication since  $q_1$  encodes the product  $x_0x_1$ . However, in practice, we prefer the dedicated multiplication circuit shown in [Fig. 1b](#), which requires only 1 CNOT gate. Therefore, since qubit  $q_1$  in [Fig. 1c](#) is no longer needed, it can be reset and reused for subsequent operations.

The **negation** operation is implemented using the standard  $X$ -gate applied to a specific qubit, as shown in [Fig. 1d](#). In some instances, negation is required to change the sign of the real input, transforming  $x \rightarrow -x$ . This technique is particularly useful for overcoming the constraint that the weight  $w$  of the weighted sum operation must be positive. By applying negation to one of the inputs, such as on qubit  $q_1$  in [Fig. 1c](#), the result becomes a weighted difference  $S_w(x_0, -x_1) = wx_0 - (1-w)x_1$ .

Finally, the random **parity flip** operation, implemented by the circuit shown in [Fig. 1e](#), is required when multiple addition operations are performed sequentially, such as constructing a polynomial [\(1\)](#). This operation must be applied after each sum operation to eliminate unwanted terms in the quantum state before the next quantum operator is executed. Notably, it is the only *non-reversible* operation among the four.

We refer to [Appendix A](#) for a detailed discussion of these arithmetic quantum circuits and their concatenation to form linear combinations.

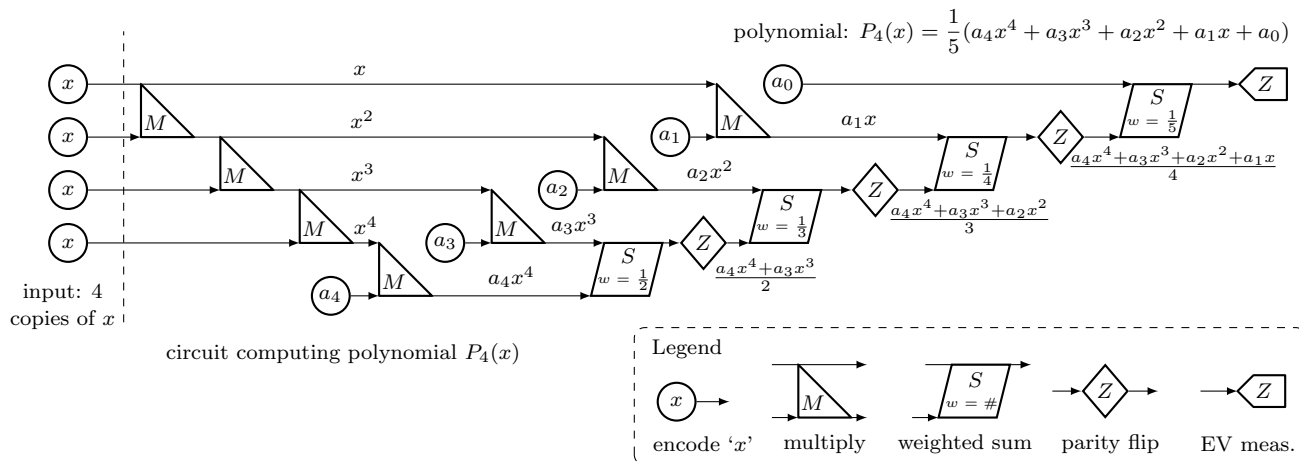


FIG. 2. **EHands protocol** for computing a degree-4 polynomial on  $x$ . The quantum circuits implementing the operations listed in the legend are shown in Fig. 1. Horizontal arrows represent qubit wires, with partial results stored at different stages, illustrating the step-by-step progression of the computation.

#### IV. POLYNOMIAL CONSTRUCTION

Based on the four arithmetic quantum operations of the **EHands protocol**, we present a constructive method for computing a degree- $d$  polynomial,  $P_d(x)$ , on a QPU. The polynomial is given by:

$$P_d(x) = \frac{1}{d+1} (a_0 + a_1x + a_2x^2 + \dots + a_dx^d), \quad (1)$$

where the input  $x$ , the polynomial coefficients  $a_i$ , and the output are all real values constrained to the range  $[-1, 1]$ .

The  $d$  copies of the real-valued input  $x$  are encoded in an **EVEN** quantum product state on  $d$  qubits. To compute  $P_d(x)$ , we construct a quantum algorithm that sequentially applies addition and multiplication operations, similar to how a polynomial is evaluated on a classical calculator. There is no unique way to achieve this construction. Our reference implementation follows a structured approach: (i) compute all powers of the input  $x$ , (ii) multiply each power  $x^k$  by its corresponding coefficient  $a_k$ , and (iii) sum the weighted terms sequentially. Since we employ the *dyadic* operation  $S_w(x_0, x_1)$ , which combines only two inputs at a time, a sequence of  $d$  such operations is needed to evaluate  $P_d(x)$ .

A complete sequence of quantum operations for computing a degree  $d = 4$  polynomial on a real number  $x$  is illustrated in Fig. 2. Due to the *no-cloning* theorem, which prohibits reusing quantum states in multiple operations, four separate copies of the input are required. However, since the multiplication operator does not alter the upper qubit, the information stored there can be reused twice, as shown in Eq. (A8) of Appendix A. The parity flip operation must be applied after each sum operator to ensure proper cancellation of unwanted quantum state components. This requires an ancilla qubit acting as a fair coin random generator. For each shot, the ancilla qubit is initialized to the  $|+\rangle$  state, measured, and

based on the measurement outcome, a  $Z$  gate is applied conditionally to a specific qubit.

The quantum resources required for this reference implementation of  $P_d(x)$  using the **EHands protocol** are: (i)  $d+1$  qubits, (ii)  $4d-1$  CNOT gates, (iii)  $3d+1$  CNOT depth, (iv)  $d$  resets, (v)  $d-1$  mid-circuit measurements with conditional gates, (vi) one final qubit measurement. It is possible to implement the same  $P_d(x)$  using a different sequence of arithmetic operations, where the circuit depth scales as  $O(\log(d))$ , but at the cost of increasing the number of qubits and CNOT gates to  $O(d^2)$ . Such trade-off between entangling gates count and qubit count may be advantageous for NISQ-era devices, which often have many available qubits but are limited by entangling gates fidelity. The implementation details of this alternative approach are beyond the scope of this paper.

The quantum implementation of  $P_d(x)$  presented in Fig. 2 is *non-reversible* because it relies on the parity flip operator, which involves multiple mid-circuit measurement. However, with some overhead it is possible to construct a *reversible* implementation of  $P_d(x)$ . Such reversible implementation requires multiple versions of the algorithm shown in Fig. 2. For each instance of the parity flip operation, marked as a diamond with  $Z$  in the figure, the entire circuit must be duplicated, with one version containing an identity gate ( $I$ ) and the other containing a  $Z$  gate. This results in a set of circuits resembling a binary tree structure. All circuits must be executed for the same number of shots, and their expectation values must be averaged to obtain the correct result. Both the reversible and non-reversible implementations of  $P_d(x)$  yield mathematically accurate results. While more resource-intensive, the reversible approach supports partially homomorphic computation, making it potentially useful for privacy-preserving quantum computation.

## V. NUMERICAL SIMULATIONS

To demonstrate the flexibility of the **EHands protocol**, we selected three common functions listed in the upper rows of [Table I](#). Each function was approximated by a polynomial of degree 5 or 6, depending on its parity, through classical pre-processing. These polynomials were then implemented as **EHands** quantum circuits by naturally extending the pattern shown in [Fig. 2](#) to the required degree  $d$ .

Those quantum circuits were simulated using the shot-based ideal Qiskit simulator for a grid of 21 equally spaced input values  $x \in [-1, 1]$ . As shown in the top panel of [Fig. 3](#), the simulated Qiskit results closely match the analytical values of each polynomial, demonstrating strong agreement and confirming the accuracy of our approach.

## VI. QUANTUM EXPERIMENTS

To further validate the **EHands protocol**, we implemented low-degree approximations of the three functions listed in the lower portion of [Table I](#). We executed the corresponding **EHands** circuits on IBM’s real quantum hardware, specifically *IBM Torino*, *Fez*, and *Marrakesh* devices. The results, shown in the bottom panel of [Fig. 3](#), demonstrate reasonable agreement with the ground truth, successfully capturing the key trend and parity of the target functions. However, the discrepancies between the results from different QPUs reflect the individual biases introduced by each NISQ device. Notably, hardware performance can vary significantly from day to day, as IBM’s compiler dynamically selects different physical qubits based on their latest calibration. The results presented in [Fig. 3](#) were obtained without applying any error correction or mitigation techniques. We have explored some error mitigation strategies, including randomized compilation [16] and noise-aware qubit selection to optimize the qubit layout [17]. However, no statistically significant improvement was observed, suggesting that intrinsic noise remains a dominant factor in these near-term quantum experiments.

## VII. DISCUSSION

The **EHands protocol** offers a versatile framework for implementing polynomial computations on QPUs, especially in the context of NISQ devices. By leveraging the **EVEN** encoding and standard quantum gates and operations, our protocol addresses a key challenge in quantum computation—efficient multivariable polynomial approximations. Experimental results confirm the feasibility of our approach on current quantum hardware, though its accuracy is currently constrained by device-specific NISQ biases. As hardware performance improves, we anticipate

TABLE I. Polynomial approximations of selected functions for testing the performance of the **EHands protocol** in both ideal simulations and real quantum hardware experiments.

target function	<a href="#">Fig. 3</a> panel	poly degree	num CNOT	dynamic range <sup>a</sup>	used shots <sup>b</sup>
<b>ideal Qiskit</b>					
$\exp(2x)$	a	5	19	0.6	3e3
$\arctan(5x)$	b	5	19	0.09	4e5
$\exp(-(3x)^2)$	c	6	23	0.015	1e6
<b>IBM QPUs</b>					
$\text{ReLU}(x)$	d	3	11	0.6	4e3
$\arctan(5x)$	e	3	11	0.3	1e4
$x^2/3$	f	2	7	0.35	1e4

<sup>a</sup>  $\max(f) - \min(f)$

<sup>b</sup> per  $x$ -data point

that even deeper circuits for higher-degree polynomials will yield reliable results.

A key advantage of the **EHands protocol** is its capability to perform *vectorized* polynomial operations. Due to space constraints, this aspect is not explored in detail here. However, by incorporating advanced data encoding schemes such as **QPIXL** [18] and **QCrank** [19], a series of  $n$  real-valued data points can be efficiently stored on a QPU using only  $\lceil \log_2 n \rceil$  additional address qubits. This integration enables *parallel computation* of the desired polynomial across entire sequences of real numbers, significantly enhancing the utility of the **EHands protocol**. Combining the **EHands protocol** with a **QCrank** encoder enables vectorized polynomial computations, making it particularly useful for non-stationary signal analysis and noise/interference reduction directly on quantum hardware. A carefully chosen polynomial can adapt to varying signal characteristics, enhancing accuracy in dynamic environments.

This capability also has significant implications for quantum machine learning (QML). The ability to perform batch processing using vectorized quantum operations makes the **EHands protocol** a valuable tool for tasks such as computing batch-average mean square error (MSE) on a QPU in ML-regression problems. Notably, the MSE, when measured as the expectation value of a single qubit, serves as a local cost function, helping to mitigate the problem of barren plateaus. Further details of the MSE implementation and its potential for enhancing quantum-assisted optimization processes are discussed in [Appendix B](#).

Beyond QML, the **EHands protocol** has promising applications in quantum image processing (QImP), where polynomial-based filters play a crucial role in edge detection and noise reduction. By integrating the **EHands protocol** with efficient encoding strategies, such as **QCrank**, these image processing tasks can be performed with enhanced computational efficiency and accuracy. This integration could drive significant advancements in

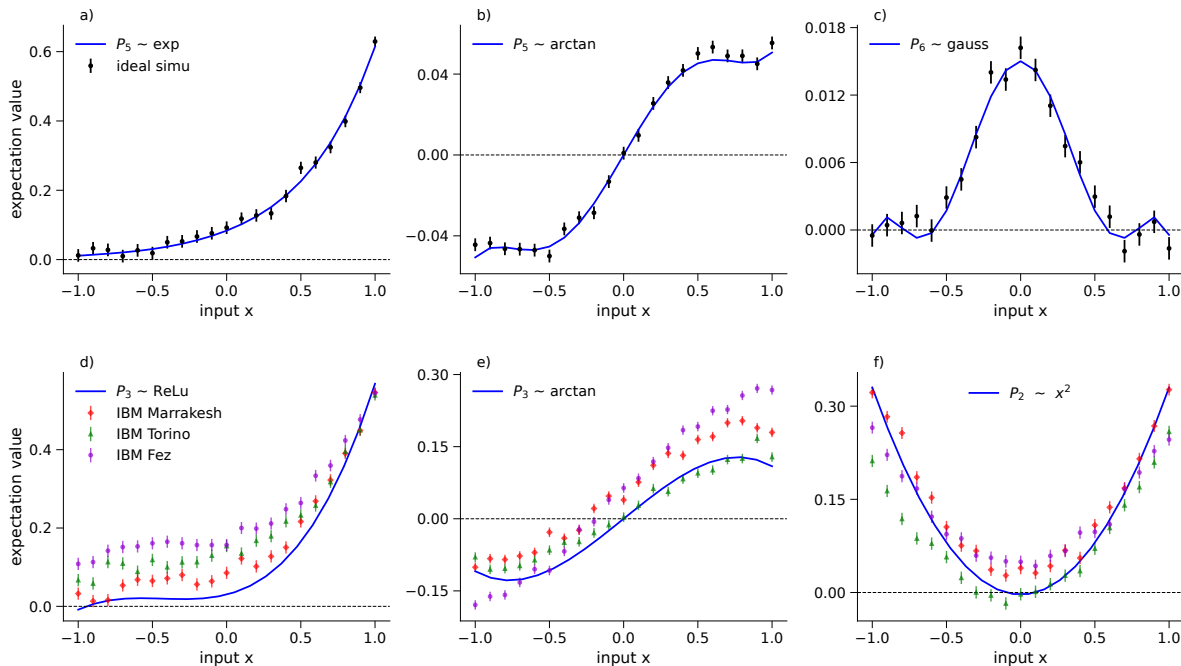


FIG. 3. (Top) Polynomial approximations of the selected functions listed in Table I are accurately reproduced by ideal Qiskit simulations. The solid curves represent the ground truth, while the data points, shown with statistical error bars, were obtained from a shot-based simulator using the number of shots specified in the last column of the table. (Bottom) Lower-degree polynomials of different parity were computed on IBM’s *Torino*, *Fez*, and *Marrakesh*. No error mitigation was applied.

quantum-enhanced image analysis pipelines.

Despite its flexibility and efficiency, the **EHands protocol** faces scalability challenges when measuring expectation values for higher-degree polynomials. Due to signal attenuation of  $O(1/d)$ , achieving accurate results requires increasing the number of measurements, which scale as  $O(d^2)$  to maintain precision. While increasing shot counts can partially address this issue, exploring amplitude amplification techniques may provide more efficient solutions.

In conclusion, the **EHands protocol** represents a significant step forward in leveraging quantum hardware for real-world applications that rely on polynomial computations. Its potential spans multiple domains, including quantum machine learning, signal processing, and image analysis, where efficient polynomial transformations are essential. As quantum hardware continues to advance, the scalability and adaptability of the **EHands protocol**

make it a promising candidate for further development and integration into more complex quantum computing frameworks.

## ACKNOWLEDGMENTS

This research was supported by the U.S. Department of Energy (DOE) under Contract No. DE-AC02-05CH11231, through the Office of Science, Office of Advanced Scientific Computing Research (ASCR) Exploratory Research for Extreme-Scale Science and Accelerated Research in Quantum Computing. This research used resources of two DOE user facilities: the National Energy Research Scientific Computing Center (NERSC) located at Lawrence Berkeley National Laboratory, operated under Contract No. DE-AC02-05CH11231, and the Oak Ridge Leadership Computing Facility, operated under Contract No. DE-AC05-00OR22725.

- 
- [1] P. W. Shor, Algorithms for quantum computation: discrete logarithms and factoring, in *Proceedings 35th Annual Symposium on Foundations of Computer Science* (1994) pp. 124–134.  
 [2] L. K. Grover, A fast quantum mechanical algorithm for database search, in *Proceedings of the 28th Annual ACM*

- Symposium on Theory of Computing* (1996) pp. 212–219.  
 [3] A. W. Harrow, A. Hassidim, and S. Lloyd, Quantum algorithm for linear systems of equations, *Phys. Rev. Lett.* **103**, 150502 (2009).  
 [4] G. H. Low and I. L. Chuang, Optimal Hamiltonian simulation by quantum signal processing, *Phys. Rev. Lett.*

- 118**, 010501 (2017).
- [5] V. Vedral, A. Barenco, and A. Ekert, Quantum networks for elementary arithmetic operations, *Phys. Rev. A* **54**, 147 (1996).
- [6] Y. Takahashi and N. Kunihiro, A linear-size quantum circuit for addition with no ancillary qubits, *Quantum Inf. Comput.* **5**, 440 (2005).
- [7] Y. Takahashi and N. Kunihiro, A fast quantum circuit for addition with few qubits, *Quantum Inf. Comput.* **8**, 636 (2008).
- [8] Y. Takahashi, Quantum arithmetic circuits: A survey, *IEICE Trans. Fundam. Electron. Commun. Comput. Sci.* **E92.A**, 1276 (2009).
- [9] S. Wang, X. Li, W. J. B. Lee, S. Deb, E. Lim, and A. Chattopadhyay, A comprehensive study of quantum arithmetic circuits, *Philos. Trans. R. Soc. A* **383**, 20230392 (2025).
- [10] G. H. Low and I. L. Chuang, Optimal Hamiltonian simulation by quantum signal processing, *Phys. Rev. Lett.* **118**, 010501 (2017).
- [11] Y. Dong, L. Lin, H. Ni, and J. Wang, Infinite quantum signal processing, *Quantum* **8**, 1558 (2024).
- [12] A. Gilyén, Y. Su, G. H. Low, and N. Wiebe, Quantum singular value transformation and beyond: exponential improvements for quantum matrix arithmetics, in *Proceedings of the 51st Annual ACM SIGACT Symposium on Theory of Computing* (2019) pp. 193–204.
- [13] Y. Dong, L. Lin, and Y. Tong, Ground-state preparation and energy estimation on early fault-tolerant quantum computers via quantum eigenvalue transformation of unitary matrices, *PRX Quantum* **3**, 40305 (2022).
- [14] E. Recio-Armengol and J. Bowles, IQPopt: Fast optimization of instantaneous quantum polynomial circuits in JAX, arXiv: 10.48550/arXiv.2501.04776 (2025).
- [15] M. Rath and H. Date, Quantum data encoding: a comparative analysis of classical-to-quantum mapping techniques and their impact on machine learning accuracy, *EPJ Quantum Technol.* **11**, 72 (2024).
- [16] J. J. Wallman and J. Emerson, Noise tailoring for scalable quantum computation via randomized compiling, *Phys. Rev. A* **94**, 052325 (2016).
- [17] P. D. Nation and M. Treinish, Suppressing quantum circuit errors due to system variability, *PRX Quantum* **4**, 010327 (2023).
- [18] M. G. Amankwah, D. Camps, E. W. Bethel, R. Van Beeumen, and T. Perciano, Quantum pixel representations and compression for N-dimensional images, *Sci. Rep.* **12**, 7712 (2022).
- [19] J. Balewski, M. G. Amankwah, R. Van Beeumen, E. W. Bethel, T. Perciano, and D. Camps, Quantum-parallel vectorized data encodings and computations on trapped-ion and transmon QPUs, *Sci. Rep.* **14**, 3435 (2024).

## APPENDIXES

In the Appendixes, we discuss in detail the derivation of the **EHands** protocol presented in the main text. In [Appendix A](#), we describe the **EVEN** encoding and decoding as well as the four key **EHands** quantum circuits for *multiplication*, *addition*, *negation*, and *parity flip*. In [Appendix B](#), we illustrate the computation of the mean squared error (MSE) with the **EHands** protocol.

### Appendix A: State vectors and observables for **EHands** protocol

#### 1. **EVEN** encoding and decoding of 2 real numbers on 2 qubits

**Encoding.** Let us consider 2 real values  $\{x_0, x_1\}$  in the range  $[-1, 1]$ . The encoding process involves mapping each value  $x_i$  to an angle  $\theta_i$ :

$$\theta_i = \arccos(x_i), \quad i = 0, 1. \quad (\text{A1})$$

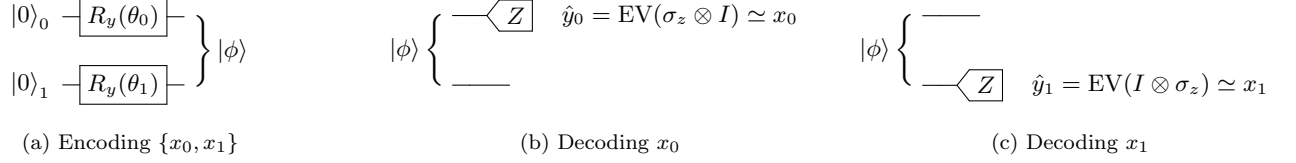
These angles parameterize rotation gates  $R_y(\theta_i)$ , which are then applied to a 2-qubit quantum state initialized in  $|00\rangle$ :

$$|\phi\rangle = [R_y(\theta_0) \otimes R_y(\theta_1)] |00\rangle = \begin{bmatrix} \cos(\theta_0/2) \cos(\theta_1/2) \\ \cos(\theta_0/2) \sin(\theta_1/2) \\ \sin(\theta_0/2) \cos(\theta_1/2) \\ \sin(\theta_0/2) \sin(\theta_1/2) \end{bmatrix} = \frac{1}{2} \begin{bmatrix} \sqrt{1+x_0} \sqrt{1+x_1} \\ \sqrt{1+x_0} \sqrt{1-x_1} \\ \sqrt{1-x_0} \sqrt{1+x_1} \\ \sqrt{1-x_0} \sqrt{1-x_1} \end{bmatrix}, \quad (\text{A2})$$

where we applied the last equality [Eq. \(A1\)](#) and relationships between trigonometric and inverse trigonometric functions. The resulting state  $|\phi\rangle$ , shown also as [Circuit 1a](#), *encodes* the classical information about  $\{x_0, x_1\}$ .

**Decoding.** In order to retrieve the values  $\{x_0, x_1\}$  encoded in the state  $|\phi\rangle$ , we define two complementary operators

$$O_s := \sigma_z \otimes I = \begin{bmatrix} 1 & 0 & 0 & 0 \\ 0 & 1 & 0 & 0 \\ 0 & 0 & -1 & 0 \\ 0 & 0 & 0 & -1 \end{bmatrix}, \quad O_p := I \otimes \sigma_z = \begin{bmatrix} 1 & 0 & 0 & 0 \\ 0 & -1 & 0 & 0 \\ 0 & 0 & 1 & 0 \\ 0 & 0 & 0 & -1 \end{bmatrix}, \quad (\text{A3})$$



CIRCUIT 1: (a) Encoding of 2 real numbers  $\{x_0, x_1\}$  in a 2-qubit state  $|\phi\rangle$ . (b)–(c) Decoding is performed by measuring the expectation value of the Pauli-Z operator on the corresponding qubit.

which represent measurements of qubit  $q_0$  and qubit  $q_1$  in the  $Z$ -basis, respectively. Next, we measure expectation values (EV) of the operators  $O_s, O_p$ , yielding back the estimators of the input values

$$\langle\phi|O_s|\phi\rangle = x_0, \quad \langle\phi|O_p|\phi\rangle = x_1. \quad (\text{A4})$$

The corresponding *decoding* quantum circuits are depicted in [Circuits 1b](#) and [1c](#), where  $\text{---}\langle Z \rangle\text{---}$  denotes measuring the EV of the corresponding qubit in the  $Z$ -basis.

## 2. Product-with-memory circuit

After establishing a method to encode and decode a pair of real values using a 2-qubit system, we introduce a unitary  $U_{\text{prod}}$  to compute their product. When  $U_{\text{prod}}$  is applied to the state  $|\phi\rangle$ , as defined in [Eq. \(A2\)](#), it produces a new state  $|\psi_{\Pi}\rangle$ . The expectation value (EV) of  $O_p$  for this state corresponds to the estimator of the product  $x_0x_1$ .

Let  $R_z(\pi/2) = e^{-i\frac{\pi}{4}} \begin{bmatrix} 1 & 0 \\ 0 & i \end{bmatrix}$ . We define the *product*-unitary  $U_{\text{prod}}$  as follows

$$U_{\text{prod}} := \text{CNOT}_{0,1} \cdot [I \otimes R_z(\pi/2)] = e^{-i\frac{\pi}{4}} \begin{bmatrix} 1 & 0 & 0 & 0 \\ 0 & i & 0 & 0 \\ 0 & 0 & 0 & i \\ 0 & 0 & 1 & 0 \end{bmatrix}. \quad (\text{A5})$$

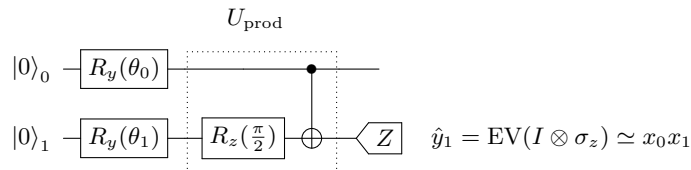
Next, by applying  $U_{\text{prod}}$  to the encoded state  $|\phi\rangle$  given in [Eq. \(A2\)](#), we obtain the state

$$|\psi_{\Pi}\rangle = U_{\text{prod}}|\phi\rangle = \frac{e^{-i\frac{\pi}{4}}}{2} \begin{bmatrix} \sqrt{1+x_0}\sqrt{1+x_1} \\ i\sqrt{1+x_0}\sqrt{1-x_1} \\ i\sqrt{1-x_0}\sqrt{1-x_1} \\ \sqrt{1-x_0}\sqrt{1+x_1} \end{bmatrix}, \quad (\text{A6})$$

so that the EV of  $O_p$  returns the product of the 2 inputs

$$\langle\psi_{\Pi}|O_p|\psi_{\Pi}\rangle = x_0x_1. \quad (\text{A7})$$

The corresponding quantum circuit is depicted in [Circuit 2](#).



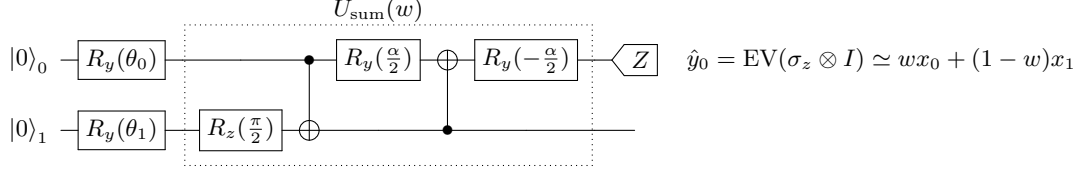
CIRCUIT 2: Computing product  $x_0x_1$  as the expectation value of  $\sigma_z$  operator measured on  $q_1$ .

Note that  $U_{\text{prod}}$  does not affect qubit  $q_0$ . As a result, this qubit retains the information about its input value  $x_0$ . Hence, the EV of  $O_s$  after applying  $U_{\text{prod}}$  remains unchanged

$$\langle\psi_{\Pi}|O_s|\psi_{\Pi}\rangle = x_0. \quad (\text{A8})$$

### 3. Weighted sum circuit

Our next goal is to compute linear combinations of a pair of real numbers. These numbers are again encoded in the 2-qubit state  $|\phi\rangle$ , as defined in Eq. (A2). To do so, we introduce the unitary  $U_{\text{sum}}$ . When  $U_{\text{sum}}$  is applied to the state  $|\phi\rangle$ , it produces a new state  $|\psi_\Sigma\rangle$ . The expectation value (EV) of  $O_s$  for this state corresponds to the estimator of the weighted sum  $wx_0 + (1-w)x_1$ , where the relative weight  $w \in [0, 1]$ . Circuit 3 encapsulates this entire process.



CIRCUIT 3: Computing weighted sum  $wx_0 + (1-w)x_1$  as EV of  $\sigma_z$  operator measured on  $q_0$ .

The unitary  $U_{\text{sum}}$  contains a rotation parameter  $\alpha$  which depends on  $w$  as follows

$$\alpha = \arccos(1 - 2w). \quad (\text{A9})$$

To prove the above, we start by expressing the rotation matrices  $R_y(\alpha/2)$  and  $R_y(-\alpha/2)$ , with  $\alpha \in [0, \pi]$ , in terms of the parameter  $w$ :

$$R_y(\pm \alpha/2) = \frac{1}{\sqrt{2}} \begin{bmatrix} \sqrt{1 + \sqrt{1-w}} & \mp \sqrt{1 - \sqrt{1-w}} \\ \pm \sqrt{1 - \sqrt{1-w}} & \sqrt{1 + \sqrt{1-w}} \end{bmatrix}, \quad (\text{A10})$$

and define the parameterized *sum*-unitary  $U_{\text{sum}}(w)$  as follows

$$U_{\text{sum}}(w) := [R_y(-\alpha/2) \otimes I] \cdot \text{CNOT}_{1,0} \cdot [R_y(\alpha/2) \otimes I] \cdot U_{\text{prod}} = e^{-i\frac{\pi}{4}} \begin{bmatrix} 1 & 0 & 0 & 0 \\ 0 & i\sqrt{w} & \sqrt{1-w} & 0 \\ 0 & 0 & 0 & i \\ 0 & i\sqrt{1-w} & -\sqrt{w} & 0 \end{bmatrix}. \quad (\text{A11})$$

Next, by applying  $U_{\text{sum}}(w)$  to the encoded state  $|\phi\rangle$  given in Eq. (A2), we obtain the state

$$|\psi_\Sigma\rangle = U_{\text{sum}}(w) |\phi\rangle = \frac{e^{-i\frac{\pi}{4}}}{2} \begin{bmatrix} \sqrt{1+x_0}\sqrt{1+x_1} \\ i\sqrt{w}\sqrt{1+x_0}\sqrt{1-x_1} + \sqrt{1-w}\sqrt{1-x_0}\sqrt{1+x_1} \\ i\sqrt{1-x_0}\sqrt{1-x_1} \\ i\sqrt{1-w}\sqrt{1+x_0}\sqrt{1-x_1} - \sqrt{w}\sqrt{1-x_0}\sqrt{1+x_1} \end{bmatrix}, \quad (\text{A12})$$

so that the EV of  $O_s$  returns the weighted sum of the 2 inputs

$$\langle \psi_\Sigma | O_s | \psi_\Sigma \rangle = wx_0 + (1-w)x_1. \quad (\text{A13})$$

Note that the first 2 gates of  $U_{\text{sum}}$  are equal to  $U_{\text{prod}}$  and the remaining gates of  $U_{\text{sum}}$  do not change  $q_1$  in Circuit 3, hence, qubit  $q_1$  contains the  $x_0x_1$  product, i.e.,

$$\langle \psi_\Sigma | O_p | \psi_\Sigma \rangle = x_0x_1. \quad (\text{A14})$$

For the special choice of  $w = 1/2 \rightarrow \alpha = \pi/2$  the result of Eq. (A13) is a plain average:  $(x_0 + x_1)/2$ .

For completeness, Table II lists other possible algebraic operations on  $x_0$  and  $x_1$  enabled by Circuit 3. These operations are obtained by measuring the qubits of the final state  $|\psi_\Sigma\rangle$  in other bases.

### 4. Linear combinations by concatenating summation circuits

We now generalize Circuit 3 to compute the linear combination of three real numbers. This generalization uses three qubits and two different  $U_{\text{sum}}$  gates. Our objective is to compute the linear combination of 3 real values  $\{x_0, x_1, x_2\} \in [-1, 1]$ :

$$s_3 = a_0x_0 + a_1x_1 + a_2x_2, \quad (\text{A15})$$

TABLE II. Expectation values for **Circuit 3** for projective single-qubit measurement in the  $X$ ,  $Y$ , and  $Z$  bases.

Measurement Basis	$\text{EV}[q_0] = \langle \psi_\Sigma   O_P   \psi_\Sigma \rangle$	$\text{EV}[q_1] = \langle \psi_\Sigma   O_P   \psi_\Pi \rangle$
$\text{---} \langle X \rangle^{\text{a}}$	$\sqrt{w(1-w)}(x_0 - x_1)$	$\sqrt{1-w} \cdot \sqrt{1-x_0^2}$
$\text{---} \langle Y \rangle^{\text{b}}$	$\sqrt{1-x_0^2} \cdot \sqrt{1-x_1^2}$	$\sqrt{w} \cdot \sqrt{1-x_1^2}$
$\text{---} \langle Z \rangle$	$w \cdot x_0 + (1-w) \cdot x_1$	$x_0 \cdot x_1$

<sup>a</sup> Measuring in the  $X$ -basis:  $\text{---} \langle H \rangle \langle Z \rangle$   
<sup>b</sup> Measuring in the  $Y$ -basis:  $\text{---} \langle S^\dagger \rangle \langle H \rangle \langle Z \rangle$

where the coefficients satisfy the following constraints

$$a_0 + a_1 + a_2 = 1, \quad a_i \in [0, 1]. \quad (\text{A16})$$

Strictly speaking, the coefficients  $a_i$  must be non-negative. However, we will later introduce a trick involving the insertion of  $X$ -gates, enabling us to also handle cases with negative coefficients as well.

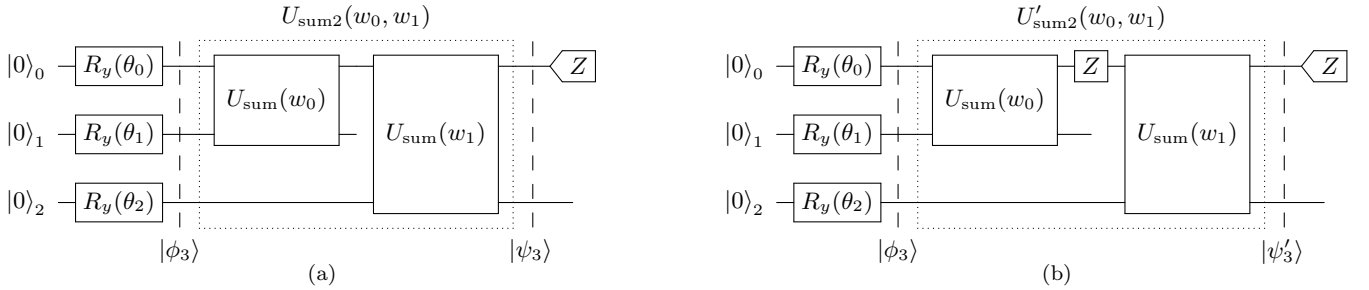
First, we need to expand the input EVEN encoding to encode 3 real values in the following 3-qubit state

$$|\phi_3\rangle = [R_y(\theta_0) \otimes R_y(\theta_1) \otimes R_y(\theta_2)] |000\rangle, \quad (\text{A17})$$

where  $\theta_i$  are given in [Eq. \(A1\)](#). Intuitively, the concatenation of two  $U_{\text{sum}}$  circuits is expect to produce

$$s_3 = w_1 [w_0 x_0 + (1 - w_0) x_1] + (1 - w_1) x_2 = \underbrace{w_1 w_0}_{a_0} \cdot x_0 + \underbrace{w_1 (1 - w_0)}_{a_1} \cdot x_1 + \underbrace{(1 - w_1)}_{a_2} \cdot x_2, \quad (\text{A18})$$

where the two  $U_{\text{sum}}$ -parameters  $w_0$  and  $w_1$  can be found by solving the set of [Eqs. \(A15\)](#) and [\(A18\)](#). A particular edge case of  $w_0 = 1/2$ ,  $w_1 = 2/3$  would result in the plain average over 3 numbers:  $(x_0 + x_1 + x_2)/3$ . The corresponding quantum circuit, shown in [Circuit 4a](#), combines  $U_{\text{sum}}(w_0)$ , acting on qubits  $\{0, 1\}$ , with  $U_{\text{sum}}(w_1)$ , acting on qubits  $\{0, 2\}$ .



CIRCUIT 4: Two circuits yielding expectation value being the sequential weighted sum of 3 input values with some ‘unwanted’ term  $f(\cdot) : \text{EV} = w_1 [w_0 x_0 + (1 - w_0) x_1] + (1 - w_1) x_2 \pm f(x_0, x_1, x_2; w_0, w_1)$ , for circuits (a) and (b), respectively.

However, after measuring qubit  $q_0$  in [Circuit 4a](#) for the operator  $O_{s3} := \sigma_z \otimes I \otimes I$  and state  $|\psi_3\rangle = U_{\text{sum}2} |\phi_3\rangle$ , the EV

$$\langle \psi_3 | O_{s3} | \psi_3 \rangle = w_1 [w_0 x_0 + (1 - w_0) x_1] + (1 - w_1) x_2 + f(x_0, x_1, x_2; w_0, w_1) \quad (\text{A19})$$

includes an additional ‘unwanted’ term  $f(\cdot)$ . Fortunately, we can construct a closely related [Circuit 4b](#), with a  $Z$ -rotation on qubit  $q_0$  inserted between the two  $U_{\text{sum}}$  operations, which yields

$$\langle \psi'_3 | O_{s3} | \psi'_3 \rangle = w_1 [w_0 x_0 + (1 - w_0) x_1] + (1 - w_1) x_2 - f(x_0, x_1, x_2; w_0, w_1). \quad (\text{A20})$$

We can prove that the same ‘unwanted’ term  $f(\cdot)$  appear again, but with its sign reversed. Therefore, averaging over both solutions will cancel out the  $f(\cdot)$  term, resulting in the intended outcome

$$\frac{\langle \psi_3 | O_{s3} | \psi_3 \rangle + \langle \psi'_3 | O_{s3} | \psi'_3 \rangle}{2} = w_1 w_0 x_0 + w_1 (1 - w_0) x_1 + (1 - w_1) x_2 = s_3. \quad (\text{A21})$$

In practice, we will use only one *feed-forward* type quantum circuit shown in [Circuit 5](#), where the middle  $Z$ -gate (acting as a parity flip operator) is toggled on or off at random. This randomness is determined by the measurement of an ancilla qubit, followed by a Hadamard gate, ensuring equal sampling of both versions of [Circuit 4](#).

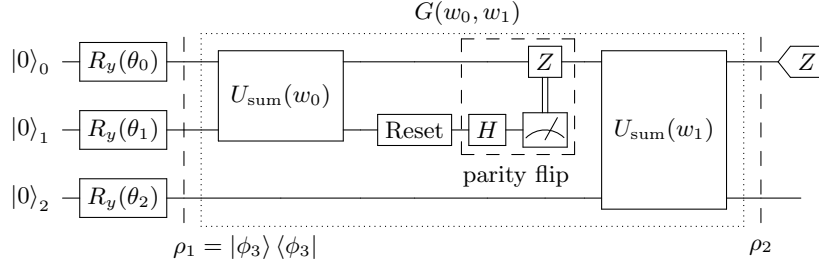
The final state resulting from [Circuit 5](#) is described by the density matrix

$$\rho_2 = \frac{G\rho_1G^\dagger}{\text{Tr}(G\rho_1G^\dagger)}, \quad (\text{A22})$$

where  $\rho_1 = |\phi_3\rangle\langle\phi_3|$  and  $G(w_0, w_1)$  the parametrized non-unitary operator defined in [Circuit 5](#). Consequently, measuring qubit  $q_0$  yields the estimator

$$\text{Tr}(O_{s3}\rho_2) = w_1w_0x_0 + w_1(1-w_0)x_1 + (1-w_1)x_2 = \hat{s}_3, \quad (\text{A23})$$

which is equal to [Eq. \(A21\)](#). In [Circuit 5](#), qubit  $q_1$  is recycled to serve as a random generator, but the protocol would work equally well if an extra ancilla qubit was used instead.



CIRCUIT 5: Dynamic circuit yielding expectation value being the sequential weighted sum of 3 input values:  $\text{Tr}(O_{s3}\rho_2) = w_1[w_0x_0 + (1-w_0)x_1] + (1-w_1)x_2$ .

Note that it is possible to obtain a modified version of [Circuit 5](#) to handle a sum with a negative coefficient  $a_j < 0$ . This can be achieved by inserting an  $X$ -gate before the  $R_y(\theta_j)$  gate for the specific input qubit  $q_j$ . It is equivalent to flipping the sign of  $x_j \rightarrow -x_j$  while using  $|a_j| > 0$  in [Circuit 5](#).

[Circuit 5](#) can be further generalized to compute a weighted sum over  $K$  inputs by concatenating  $K-1$   $U_{\text{sum}}$  unitaries, interspersed with  $K-2$  random  $Z$ -gates. For any set of desired coefficients  $a_i$ , it is always possible to determine  $K-1$   $U_{\text{sum}}$ -parameters  $w_j$ . A plain average over  $K$  variables:  $\frac{1}{K} \sum_{i=0}^{K-1} x_i$  can be obtained using weights:  $w_i = \frac{i+1}{i+2}$  for  $i \in [0, \dots, K-2]$ .

## Appendix B: Computation of Mean Squared Error with EHands protocol

The mean squared error (MSE) is widely used in machine learning to evaluate the performance of regression models. It measures the average squared differences between the true values  $y_i$  and predicted values  $x_i$ , helping assess model accuracy and guiding optimization processes. The MSE is defined as:

$$\text{MSE}(\mathbf{x}, \mathbf{y}) = \frac{1}{N} \sum_{i=0}^{N-1} (x_i - y_i)^2,$$

where  $N$  is the number of predicted values.

The **EHands protocol** can be used to compute the MSE on a QPU as illustrated in [Fig. 4](#) for  $N=2$ , two pairs of real values,  $[x_0, x_1]$  and  $[y_0, y_1]$ . Each circle represents a qubit initialized to the value indicated inside it, hence the whole circuit requires 8 qubits. All elementary operations have been already defined in the main paper in [Circuit 1](#). For this MSE implementation, the total CNOT count is 12 and the CNOT depth is 5. There are 3 parity-flip operators (diamonds) which reuse 3 qubits, so this circuit calls for 3 resets and 3 mid-circuit measurements. The measurement of one qubit (pentagon) provides the output. The computation proceeds as follows:

- First, the difference between each pair of values  $(x_0 - y_0)$  and  $(x_1 - y_1)$  is calculated, twice. We negate all  $y$ -inputs so despite we use the sum operator with weight  $w = 1/2$  the results is the difference.
- The two independent copies of the differences are multiplied, yielding the terms  $(x_0 - y_0)^2$  and  $(x_1 - y_1)^2$ .

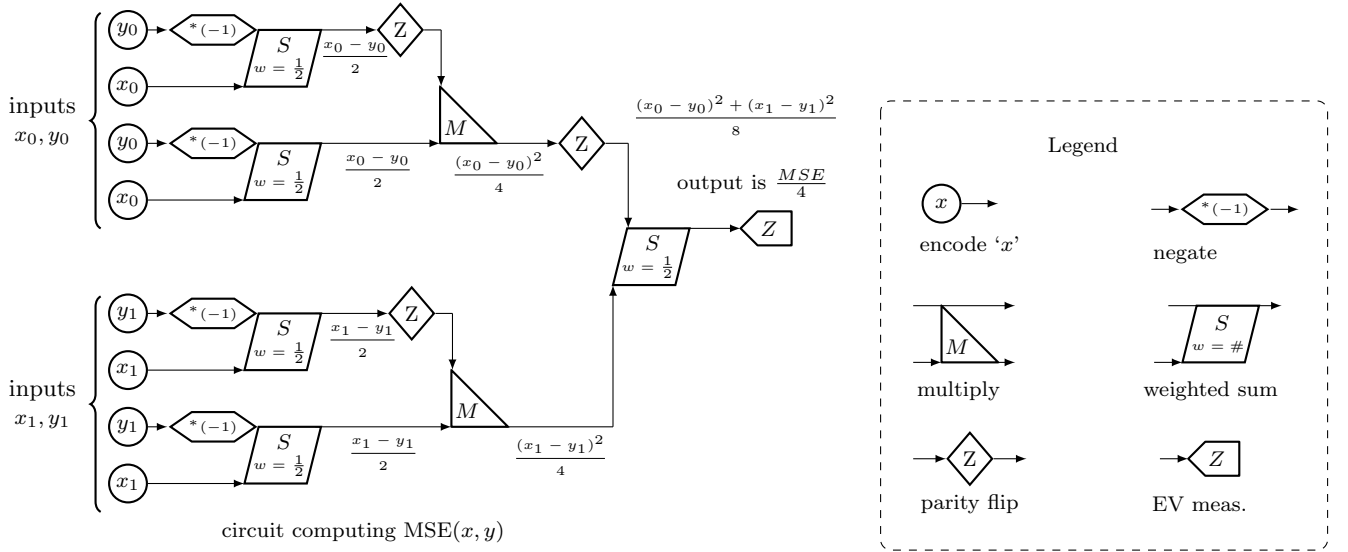


FIG. 4. **EHands** computation of mean squared error (MSE) on two pairs of real values  $[x_0, x_1]$  and  $[y_0, y_1]$ . The explicit implementation of the operations listed in the legend are defined in Fig. 1 in the main text.

- Finally, the two squared terms are averaged, resulting with the MSE which can be measured as the expectation value of qubit 2, counting from 0. Technically speaking, we measure expectation value for the operator  $O' = I^2 \otimes \sigma_z \otimes I^5$ .

The two copies of each input are necessary, because the *no-cloning* theorem prohibits using same quantum state twice, what is needed to square the values of the differences. Notice that the final output is  $MSE/4$  which is a characteristic feature of the **EHands** protocol, due to how the square of the difference is computed. This attenuation factor of 4 remains unchanged as the number of input variables ( $N$ ) increases. For the purpose of minimization, a constant scaling of the loss does not pose a problem. However, in practice, more shots are required to achieve a given statistical accuracy for the MSE.

To summarize, the MSE calculation over  $N = 2$  pairs shown in Fig. 4 involves encoding the input values  $x_0, y_0$  and  $x_1$  and  $y_1$  on 8 qubits, performing negation, weighted sums, and multiplication operations, as well as applying the parity-flip operator to ensure accuracy of the final result. The protocol can be expanded for larger number of variables ( $N > 2$ ) at the expense of  $4N$  qubits by appropriately extending the quantum circuit shown in Fig. 4.

In general, the quantum resources required to compute MSE for  $N$  inputs using the **EHands** protocol and serial sum implementation are as follows: (i)  $4N$  qubits, (ii)  $7N$  CNOT gates, (iii)  $2N + 3$  CNOT depth, (iv)  $2N - 1$  resets and mid-circuit measurements, (v) one qubit measured at the end.

Finally, one can combine the **EHands** protocol with the **QCrank** encoding to compute the average MSE over a list of  $K$  samples:  $\{x_i, y_i\}_j$  where  $i \in [N], j \in [K]$ . For this scenario all input data are stored in a single circuit which requires  $4N + \log_2(K)$  qubits and returns single real number with the  $MSE/4$  averaged over  $k$  samples. The potential application of vectorized MSE computation using the **EHands** protocol with the **QCrank** encoding include, for example, the computation of batch-average loss for QML applications or edge detection for gray-scale images on a QPU.

### 1. Polynomial in multiple variables

The **EHands** protocol can also be extended to compute polynomials involving multiple variables. Consider a polynomial  $p(x_1, x_2, \dots, x_n)$  of degree  $d$ , which can be expressed as:

$$p(x_1, x_2, \dots, x_n) = \sum_{i=0}^d a_i x_1^{i_1} x_2^{i_2} \dots x_n^{i_n},$$

where  $a_i$  are real coefficients, and each term  $x_1^{i_1} x_2^{i_2} \dots x_n^{i_n}$  represents a product of the input variables raised to different powers, with  $i_1 + i_2 + \dots + i_n \leq d$ . All input values  $x_i$  and coefficients  $a_i$  are constrained to the range  $[-1, 1]$ , ensuring that the polynomial terms are bounded and computable within the limits of the **EHands** protocol.

One potential application of computing multiple variable polynomials is in QML for computing non-linear activation function on QPU, for example.